processes

MDPI

Article

Pre-Crosslinked Gel Particles Enhanced by Amphiphilic Nanocarbon Dots in Harsh Reservoirs: Synthesis and Deep Stimulation Mechanism

Guorui Xu [1,2,3], Xiaoxiao Li [1,2,3,*], Jinzhou Yang [1,2,3], Chunyu Tong [1,2,3], Xiaolong Wang [1,2,3] and Tengfei Wang [4,*]

[1] Tianjin Key Laboratory of Offshore Difficult to Recovery Reserves Exploitation, Tianjin 300452, China; xugr@cosl.com.cn (G.X.); yangjzh14@cosl.com.cn (J.Y.); tongchy2@cosl.com.cn (C.T.); wangxl151@cosl.com.cn (X.W.)
[2] Production Optimization, China Oilfield Service Limited, Tianjin 300452, China
[3] State Key Laboratory of Offshore Oil Exploitation, Tianjin 300452, China
[4] College of Chemistry & Environmental Engineering, Yangtze University, Jingzhou 434000, China
* Correspondence: lixx49@cosl.com.cn (X.L.); wangtengfeiforever@126.com (T.W.)

Abstract

To address the issues of easy degradation, dehydration, and insufficient deep plugging strength of traditional pre-crosslinked gel particles (PPGs) in high-temperature and high-salinity reservoirs, this study innovatively introduced amphiphilic carbon dots (CDs) with both hydrophilic and hydrophobic structures as multifunctional modifiers. The carbon dot-reinforced PPGs (CD-PPGs) were successfully prepared through in situ polymerization. Through systematic characterization, microscopic visualization experiments, and macroscopic oil displacement evaluation, the performance enhancement mechanism and profile control behavior were deeply explored. The results show that the amphiphilic carbon dots significantly enhanced the material's temperature resistance (up to 110 °C), salt resistance (up to 15 × 10^4 mg/L salinity), and mechanical properties by constructing a "hydrogen bond-hydrophobic association" dual crosslinking system within the PPG network. More importantly, it was found that CD-PPGs exhibit a unique "self-aggregation" ability in deep reservoirs, which enables the in situ formation of high-strength plugging micelles at the target location while ensuring excellent injectability. At a permeability range of 539.0–2988.6 mD, the sealing rate of 0.5 PV CD-PPGs was greater than 95%. With permeabilities of 490.1 mD and 3020.5 mD under heterogeneous reservoir simulation conditions, the total recovery degree after the CD-PPGs was displaced was 52.6%, which was 20.5% higher than that of single water flooding. This study not only developed a high-performance profile control nanomaterial but also elucidated its strengthening mechanism, providing new insights and a theoretical basis for advancing deep profile control technology.

Keywords: pre-crosslinked gel particles; amphiphilic carbon dots; self-aggregation; high-temperature and high-salt reservoirs; enhanced oil recovery

check for updates

Academic Editor: Zheng Sun

Received: 18 November 2025
Revised: 5 December 2025
Accepted: 8 December 2025
Published: 10 December 2025

Citation: Xu, G.; Li, X.; Yang, J.; Tong, C.; Wang, X.; Wang, T. Pre-Crosslinked Gel Particles Enhanced by Amphiphilic Nanocarbon Dots in Harsh Reservoirs: Synthesis and Deep Stimulation Mechanism. *Processes* **2025**, *13*, 3994. https://doi.org/10.3390/pr13123994

Copyright: © 2025 by the authors. Licensee MDPI, Basel, Switzerland. This article is an open access article distributed under the terms and conditions of the Creative Commons Attribution (CC BY) license (https://creativecommons.org/licenses/by/4.0/).

1. Introduction

With the continuous growth of the global energy demand and the gradual depletion of conventional oil and gas resources, the efficient development of harsh reservoirs with high temperatures and high salinity has become an important strategic direction for ensuring national energy security. Such reservoirs typically undergo long-term water injection development and enter a high-water-cut period, during which the inherent strong

heterogeneity of the reservoir becomes increasingly pronounced [1–3]. The permeability differences formed in the reservoir due to sedimentation, diagenesis, and later tectonic movements cause the injected fluid to circulate ineffectively along high-permeability channels for a long time, seriously restricting the expansion of water flooding sweep volume and leaving a large amount of remaining oil trapped in low-permeability areas, which seriously affects the effect of reservoir fracturing and the final recovery rate. Therefore, achieving flow direction control and improving displacement efficiency in the deep part of the reservoir, i.e., deep profile control and displacement, are crucial to overcoming a development bottleneck in high-temperature and high-salinity reservoirs [4–6].

Among various profile control and displacement agents, pre-crosslinked gel particles (PPGs) have received extensive attention and application due to their advantages, including high gelation reliability, strong shear resistance, and reduced susceptibility to the compatibility of formation minerals and fluids [7–9]. However, in the face of the harsh conditions of many oil fields in China, such as high temperatures (>110 °C) and high salinity (>10×10^4 mg/L), traditional PPGs have two major bottleneck problems: (1) Insufficient stability of the body: High temperatures will intensify the thermal motion and chemical degradation of polymer molecules, and high-valent metal ions will severely compress the double electric layer on the surface of PPGs, causing them to dehydrate and shrink and lose their profile control and displacement function. (2) The contradiction between deep plugging strength and injectability: Small-sized particles designed for good injectability often cannot effectively block larger pores and holes when they reach deep formations due to their small size; that is, “injectability” and “plugging strength” are difficult to balance [10–12].

The rise of nanotechnology provides new ideas for solving the above problems. Carbon dots (CDs), as a new type of fluorescent carbon nanomaterial, have shown great potential in energy, biology, and catalysis due to their small size, large specific surface area, rich surface functional groups, and easy modification [13–15]. Inspired by this, this work designs an amphiphilic carbon dot and introduces it as a multifunctional nanomodifier into the synthesis of PPG. We expect that the amphiphilic carbon dots can not only serve as physical crosslinking points to enhance the stability of the PPG network but also, by virtue of their unique hydrophilic–lipophilic balanced structure, endow PPGs with excellent “intelligent behavior”—that is, maintaining a dispersed state during injection to ensure injectability, and upon reaching the target area and remaining there, they can self-agglomerate under the trigger of the external environment (such as temperature), thereby achieving “self-amplification” of the plugging strength at the required location [16–18].

Based on this, this work is dedicated to designing and synthesizing carbon dots with a clear amphiphilic structure and utilizing them as the basis for preparing a new generation of intelligent PPG (CD-PPG). Through comprehensive structural characterization and performance testing of CD-PPG, the intrinsic mechanism of its performance enhancement is clarified. Physical simulation experiments of sand-filled tubes are conducted to quantitatively evaluate the deep profile control and displacement effect, as well as the enhanced oil recovery capacity of the CD-PPG system under simulated reservoir conditions. The results of this work are expected to provide innovative material solutions and a solid theoretical basis for overcoming the technical bottlenecks of enhanced oil recovery in harsh reservoirs (high-temperature and high-salt).

2. Materials and Methods

2.1. Main Reagents and Instruments

2.1.1. Reagents

Reagents include acrylamide (AM, analytical purity), 2-acrylamido-2-methylpropanesulfonic acid (AMPS, analytical purity), N,N′-methylene bisacrylamide (MBA, chemical purity), ammonium persulfate (APS, analytical purity), citric acid (analytical purity), dodecylamine (analytical purity), sodium chloride, calcium chloride (both analytical purity, used for preparing simulated formation water), simulated crude oil (with certain viscosity), anhydrous ethanol, and deionized water.

2.1.2. Instrumentation and Equipment

(1) The following synthesis and processing equipment was used: microwave reactor (for carbon dot synthesis), heat-collecting constant-temperature magnetic stirrer, precision electronic balance, vacuum drying oven, high-speed grinder, and standard inspection sieve.
(2) In addition, the characterization equipment included a Fourier transform infrared spectrometer (FT-IR, VERTEX70), scanning electron microscope (SEM, ZEISS EV0MA15), thermogravimetric analyzer (TGA, STA449 F3), laser particle size analyzer, and advanced rotational rheometer.
(3) Oil displacement experimental equipment: Constant temperature box, sand-filling tube model (stainless steel, length 60 cm, inner diameter 2.5 cm), double plunger constant-speed pump, pressure data acquisition system, liquid collection and measurement device [19,20].

2.2. Preparation of Amphiphilic Carbon Dots (A-CDs)

The improved microwave-assisted solvothermal method was adopted. The procedure is as follows: accurately weigh 2.10 g of citric acid and 2.41 g of dodecylamine in a beaker, add 20 mL of deionized water, and stir with a magnetic stirrer until complete dissolution and clarity. Transfer the mixed solution to the inner lining of the microwave reactor, seal it, and place it in the microwave reactor. Maintain at 180 °C for 30 min. After the reaction, let it cool naturally to room temperature, obtaining a brownish A-CDs crude solution. Subsequently, transfer this crude solution to a pre-treated dialysis bag (with a molecular weight cut-off of 1000 Da) and perform dialysis in deionized water for 48 h to remove unreacted small molecules. Finally, freeze-dry the pure A-CDs solution, obtaining a brownish spongy solid. Grind it and store it in a desiccator for future use [21,22].

2.3. Synthesis and Optimization of CD-PPG

This study employed an integrated synthesis process of aqueous solution polymerization, in situ compounding, and freeze grinding. The specific steps are as follows:

In a 250 mL three-necked flask, 100 mL of deionized water was added, and the monomers were weighed according to a molar ratio of AM to AMPS of 7:3, with the total monomer concentration controlled at 28 wt%. The monomers were completely dissolved under an ice-water bath and continuous stirring. A total of 0.4 wt% of A-CD powder was added to the above solution, and then it was ultrasonicated in an ultrasonic disperser at a power of 400 W for 40 min to form a uniform and stable precursor dispersion solution. An appropriate amount of crosslinking agent MBA (0.05 wt% of the total mass) was added, and the mixture was stirred for another 30 min [23–25]. Subsequently, high-purity nitrogen gas was continuously introduced into the system for 45 min to completely remove dissolved oxygen. The three-necked flask was transferred to a 45 °C constant temperature water bath. After the system temperature was balanced, the initiator APS solution (0.08 wt%

of the total mass) was added all at once. The reaction was carried out under nitrogen protection for 6 h, then the temperature was raised to 60 °C for 2 h to gel, resulting in a colorless, transparent, highly resilient blocky composite gel. The gel block was immersed in liquid nitrogen for deep freeze-crystallization treatment. Immediately after that, it was crushed using a high-speed grinder and screened through a standard inspection sieve to obtain particles of 100–120 mesh. The wet particles were repeatedly washed with a 70% ethanol solution three times to remove residual monomers. Finally, the washed particles were placed in a 50 °C vacuum drying oven to dry to constant weight, resulting in the final CD-PPG product. As a blank control, the ordinary PPGs (denoted as C-PPGs) were synthesized identically without adding A-CDs [26–30].

2.4. Characterization and Testing Methods

(1) SEM observation: After the sample was fully swollen and quenched with liquid nitrogen, it was subjected to a gold-spraying treatment and then observed for its internal microstructure under a 15 kV acceleration voltage.

(2) Thermal stability analysis (TGA): In the presence of a nitrogen gas flow (50 mL/min), the sample was heated at a rate of 10 °C/min from room temperature to 800 °C, and the change in sample mass with temperature was recorded.

(3) Expansion and temperature/alkali resistance performance test: We accurately weighed 0.100 g (denoted as Wd) of the dry CD-PPG and C-PPG, and immersed them, respectively, in different mineralization degrees (fresh water, 5×10^4 mg/L, 10×10^4 mg/L, 15×10^4 mg/L NaCl/$CaCl_2$ mixed salt water (with Ca^{2+} concentration fixed at 500 mg/L)). We took them out regularly, dried the surface free of water with filter paper, and weighed them again (denoted as Ws). The expansion ratio (Q) calculation formula is $Q = (Ws - Wd)/Wd$. At the same time, we placed the fully swollen samples in a constant temperature oven at 95 °C for a long-term aging experiment. We regularly observed and recorded their morphological and weight changes [31].

(4) Texture analyzer analysis: The test was conducted using the CT3 texture analyzer from Brookfield USA. The main body gel blocks were cut into cuboid pieces with dimensions of 100 mm × 80 mm × 20 mm. To ensure uniform force application, the surface of the samples had to be flat, smooth, and free of visible bubbles or defects. The compression and TPA tests were carried out under indoor conditions (room temperature 15 °C, relative humidity 38%).

(5) Particle steady-state viscoelasticity: During the migration process in the formation, the actual shear stress direction that PPGs were subjected to by the porous medium of the formation remained unchanged. The elastic behavior exhibited under such conditions is referred to as the steady-state viscoelasticity of PPGs. The steady-state viscoelasticity of particles can reflect the actual viscoelasticity of the viscoelastic particle system during the migration process in the formation. Steady-state rate scanning experiments were conducted using a rotational rheometer to determine the elastic behavior of viscoelastic particles during the steady-state shear process. The main indicators used for characterization were the normal stress difference (N1) and the Wiesenberg number. The concentration of viscoelastic particles was 0.2%, and the test temperature was 85 °C [32,33].

The magnitude of the normal stress difference is the main manifestation of the elastic behavior of viscous elastic fluids during flow. The normal stress difference was divided into the first normal stress difference and the second normal stress difference. Due to the very small second normal stress difference in the oil-displacing viscoelastic particle solution, the current evaluation of the elasticity of the viscoelastic particle steady flow under the oil-displacing condition mainly relies on the first normal stress difference. The

description of the Wiesenberg effect of the viscoelastic particle solution can be expressed by the Wiesenberg number, which reflects the relative size of the solution's elasticity. When We is large, the flow characteristics are mainly determined by the first normal stress difference, that is, elasticity plays a dominant role; when We is small, the flow characteristics are mainly determined by the viscous force. Thus, through We, the roles of elasticity and viscosity in the viscous elastic fluid during the flow process can be known [34,35].

2.5. Plugging Performance Test

Plugging experiments were conducted using a single sand-filling pipe model to evaluate the injection performance and deep-seated sealing performance of PPGs. The length of the sand-filling pipe used in the experiment was 0.6 m, and its diameter was 2.5 cm. The basic parameters are shown in Table 1. The simulated formation water used in the experiment had a salinity of 150,000 mg/L and a temperature of 110 °C. The sand-filling pipe was saturated with water, and the permeability was measured. Then, 0.5 PV of the dispersion liquid of C-PPG and CD-PPG with a mass fraction of 0.2 wt% was injected. Every 0.05 PV, the pressure change at the injection end of the sand-filling pipe and the production volume at the outlet end were recorded, and the pressure gradient, resistance factor, and sealing rate were calculated. The experiment was stopped after the pressure stabilized following subsequent water injection [36,37].

Table 1. Basic parameters of single sand-filling pipe model.

Gel Particles	Foam Agent Mass Fraction/wt%	Injection Rate/(mL/min)	Porosity/%	Permeability/mD
C-PPG	0.2	1	30.8	1073.1
		1	33.2	3014.6
CD-PPG	0.2	1	30.7	1009.3
		1	33.6	2988.6

2.6. Water Control Flooding Experiment for Oil Recovery

The CD-PPG water control flooding effect was evaluated using a dual-tube sand-filling model (to simulate heterogeneous reservoir conditions). Sand-filled tubes with different permeabilities were connected in parallel. The injection rate was set at 1 mL/min. After water flooding for 0.9 PV, 0.5 PV of the CD-PPG dispersion liquid (with a mass fraction of 0.2%) was injected. Then, 0.8 PV of secondary water flooding was carried out. The water production rate, oil production rate, and pressure changes at the outlet end were recorded to evaluate the oil displacement effect of CD-PPGs under the simulated heterogeneous reservoir conditions. The basic parameters of the dual-sand-filling tube model are shown in Table 2 [26,38].

Table 2. T Basic parameters of double sand-filling pipe models.

Reservoir Model	Porosity/%	Permeability/mD
High-permeability tube	35.6	3020.5
Low-permeability tube	28.9	490.1

3. Experimental Results and Discussion

3.1. Characterization of Amphiphilic Carbon Dots (A-CDs)

The transmission electron microscope (TEM) results show that the synthesized A-CDs are nearly spherical in shape, with good monodispersity, and the average particle size is approximately 2.3 nm [15,39]. A transmission electron microscope image of A-CDs is shown in Figure 1.

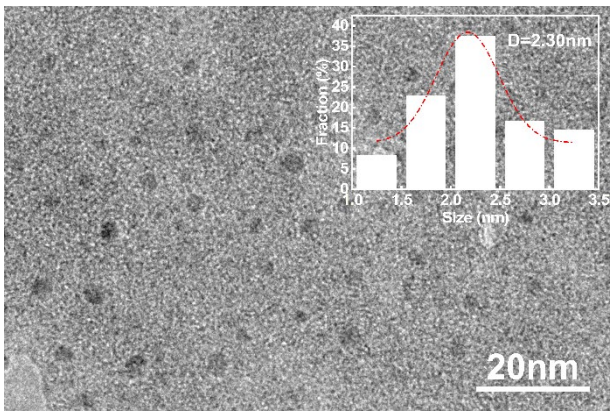


Figure 1. Transmission electron microscope image of A-CDs.

The FT-IR spectrum confirmed that the surface of the A-CDs simultaneously contained hydrophilic functional groups (such as -OH/-COOH) and hydrophobic long-chain alkanes, successfully achieving the expected amphiphilic structure [34]. The FT-IR spectrum of the A-CDs is shown in Figure 2.

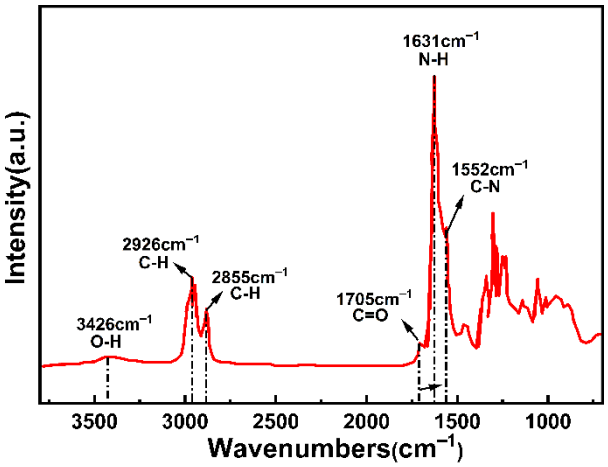


Figure 2. The FT-IR spectrum of the A-CDs.

3.2. Structural Characterization and Formation Mechanism of CD-PPGs

The SEM and microscopic morphology analysis results of CD-PPGs are shown in Figure 3. The SEM images provide compelling morphological evidence. C-PPGs show a relatively loose and non-uniform three-dimensional network structure. CD-PPGs exhibit a significantly denser and more uniform honeycomb-like or porous structure [11,40].

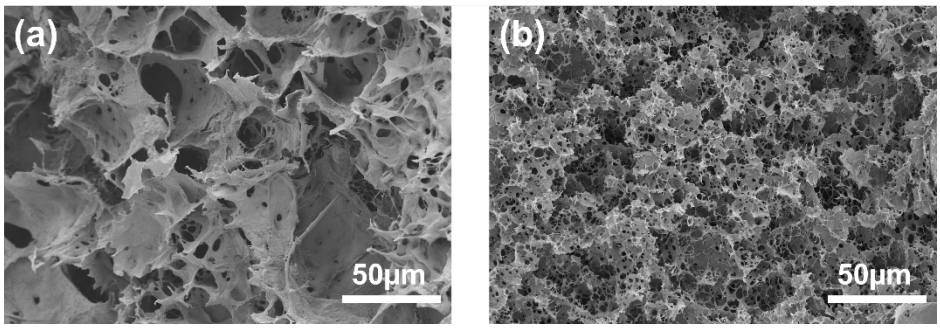


Figure 3. The results of SEM and microscopic morphology analysis.

Mechanism explanation: A-CDs play multiple crucial roles in the polymer system: ① Nano-enhancing core. The solid core of A-CDs can serve as an ideal nano-filler, directly

enhancing the polymer matrix. ② Multifunctional physical crosslinking center. Hydrogen bond crosslinking: The numerous functional groups, such as carboxyl and amino groups, on the surface of A-CDs form a dense hydrogen bond network with the amide and sulfonic acid groups on the P(AM-AMPS) molecular chains. Hydrophobic association crosslinking: The hydrophobic termini of A-CDs and the hydrophobic microregions induced by them can generate strong hydrophobic association interactions. The synergistic effect of these two mechanisms jointly constructs a robust and stable "dual crosslinking network". This structure is the primary reason for the excellent temperature resistance, salt resistance, and mechanical properties of CD-PPGs [41].

3.3. Systematic Evaluation of Thermal Resistance, Salt Resistance, and Mechanical Properties

3.3.1. Thermal Stability (TGA)

The TGA curve clearly shows that the initial thermal decomposition temperature of the C-PPGs is 274.1 °C. The initial decomposition temperature of the CD-PPGs is as high as 315.2 °C, and the residual carbon content at 600 °C is also significantly higher than that of the C-PPGs. This incontrovertibly proves that the introduction of A-CDs greatly improved the thermal stability of PPGs [14]. The TGA test results of C-PPGs and CD-PPGs is shown in Figure 4.

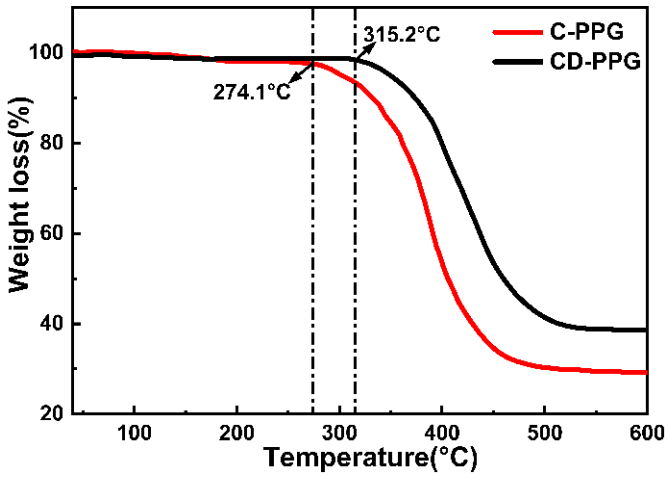


Figure 4. The TGA test graphs of C-PPGs and CD-PPGs.

3.3.2. Salt-Tolerance and Temperature Tolerance Properties

(1) Salt-tolerance at room temperature

In freshwater, the equilibrium expansion multiples of C-PPGs and CD-PPGs are similar (approximately 10 times). However, in 10×10^4 mg/L of highly mineralized salt water, the expansion multiple of C-PPGs drops sharply to approximately 4 times, showing severe salt sensitivity. In contrast, CD-PPGs can still maintain an expansion capacity of about 8 times in the same salt water, demonstrating excellent salt resistance. The evaluation results of the normal-temperature salt resistance of C-PPGs and CD-PPGs are shown in Figure 5 [19].

(2) Long-term stability at high temperatures

The samples were placed in an extreme environment of 110 °C and a mineralization degree of 15×10^4 mg/L for a 14-day aging test. The C-PPGs showed significant shrinkage, fragmentation, and even dissolution. However, after 3 days of aging, the CD-PPGs began to aggregate into particle clusters, forming viscoelastic gels. The formed gels have excellent viscoelastic properties and can enhance the sealing ability of the particle system in porous media. This "self-aggregation" ability of CD-PPGs can, under the premise of ensuring excellent injectability, form high-strength sealing clusters in the target location in

situ, effectively resolving the contradiction between injectability and sealing ability of the particle-based sealing agent [42].

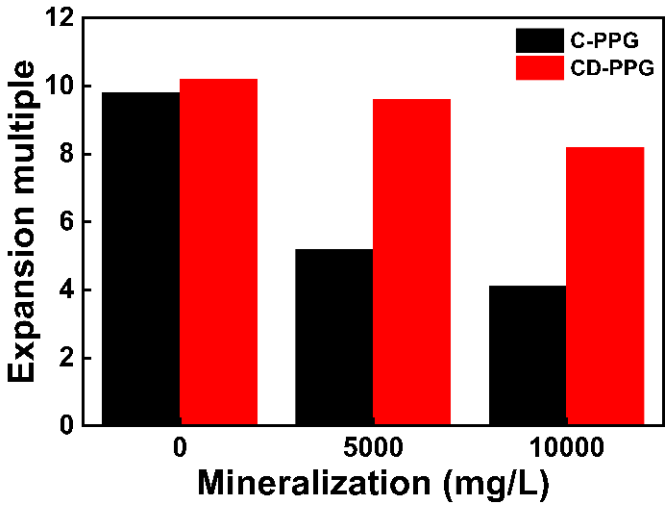
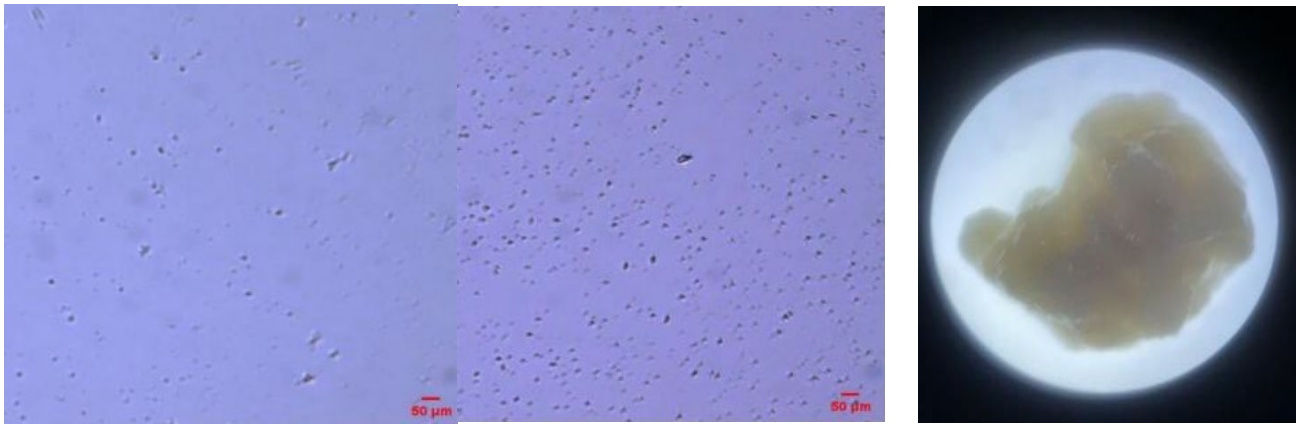


Figure 5. The evaluation results of the normal-temperature salt resistance of C-PPGs and CD-PPGs.

The evaluation results of the long-term stability under high temperatures of C-PPGs and CD-PPGs are shown in Figure 6.



(**a**) C-PPGs aged for 7 days (**b**) CD-PPGs aged for 7 days (**c**) CD-PPGs self-agglomerate to form micelles

Figure 6. The evaluation results of long-term stability under high temperatures of C-PPGs and CD-PPGs.

3.3.3. Mechanical Properties of the Matrix Adhesive

The mechanical properties of the bulk gel blocks of two types of particles were measured using a texture analyzer. The results are shown in Table 3. Since the addition of the A-CD cores can effectively dissipate mechanical energy, the fracture stress, elastic modulus, and toughness of the gel structure of the CD-PPG bulk gel significantly increased [33].

Table 3. The influence of A-CDs on the compression performance of the matrix adhesive.

Type of the Main Body Adhesive Block	Fracture Strain/%	Breaking Stress/MPa	Elasticity Modulus/MPa	Tenacity/(MJ·m^{-3})
CD-PPG	79.37	11.91	14.23	10.76
C-PPG	64.42	2.66	11.78	5.46

3.3.4. CD-PPG Steady-State Viscoelasticity

Based on the comparison experiment results of the first normal stress difference and the Wenzinger number of two types of particles, it can be seen that both the N1 representing

the elasticity of CD-PPGs and the Wenzinger number We, reflecting the relative size of the solution's elasticity, have significantly increased compared to C-PPGs. This indicates that CD-PPGs have higher elasticity during the formation movement process and have a stronger sealing ability compared to conventional viscoelastic particles [18,30]. The influence of A-CDs on the compression performance of the matrix adhesive is shown in Table 4.

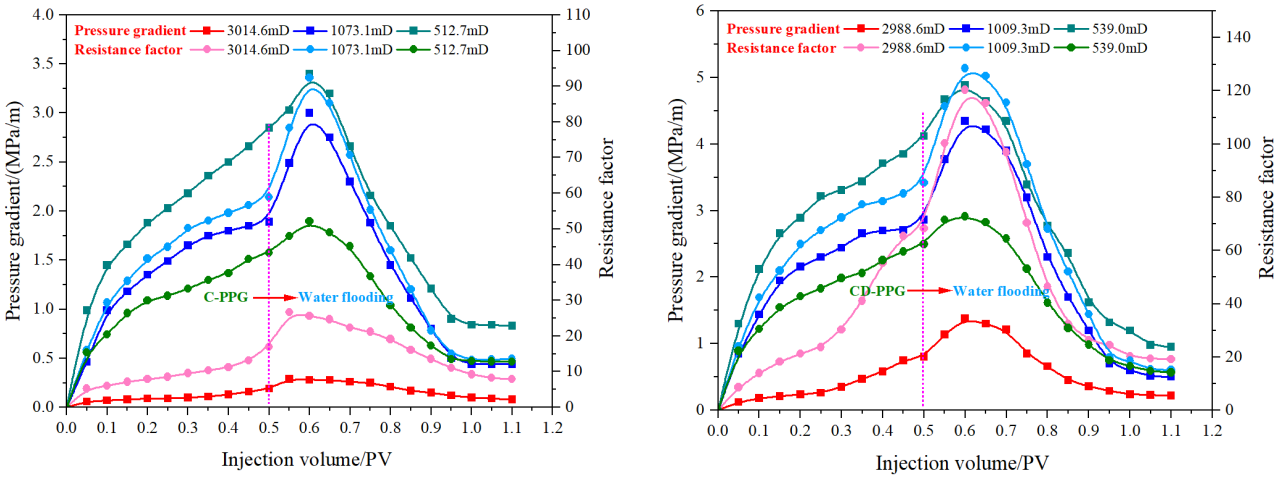
Table 4. The comparison results of the N_1 and the We for the two types of particles.

Particle Type	N1/kPa	We
CD-PPG	132	0.51
C-PPG	35	0.22

3.4. Comprehensive Evaluation of Blocking and Oil Expulsion Effects

3.4.1. Plugging Performance

The relationship curves of pressure gradient, resistance factor, and injection volume for the two types of particles under different permeabilities are shown in Figure 7. As can be seen from Figure 7a, under the simulated reservoir conditions with permeabilities of 1073.1 mD and 3014.6 mD, after injecting 0.5 PV of C-PPGs with a mass fraction of 0.2 wt%, the breakthrough pressure gradient and resistance factor were 1.89 MPa/m and 0.19 MPa/m and 58.93 and 16.96. In contrast, after injecting 0.5 PV of CD-PPGs with a mass fraction of 0.2 wt%, the breakthrough pressure gradient and resistance factor were higher, reaching 2.86 MPa/m and 0.80 MPa/m and 85.43 and 68.32. After injecting CD-PPGs, it was found that the resistance factor increased significantly after water flooding was initiated. CD-PPGs migrated towards the deeper part of the reservoir through compression deformation and achieved secondary sealing, and their anti-erosion stability was very good [28,42].



(**a**) C-PPGs (**b**) CD-PPGs

Figure 7. Pressure gradient and resistance factor curves with injection volume under varying permeabilities.

Under the simulation reservoir conditions of permeabilities of 3014.6 mD and 2988.6 mD, after injecting CD-PPGs with a mass fraction of 0.2 wt% and 0.5 PV, the sealing rate reached over 95%. The sealing performance met the production adjustment and increase requirements for high water cut blocks in offshore oil fields [34,40].

Pre-crosslinked gel particles form a stable three-dimensional network during the synthesis stage under the combined effect of surface crosslinking agents and internal network structures. This design enables them to mainly undergo elastic deformation

rather than structural rupture when subjected to high shear pumping in the wellbore and near-wellbore regions, thereby avoiding the risk of near-wellbore blockage caused by excessive crosslinking or shear degradation during injection. When the particles migrate to the target deep reservoir area, they moderately hydrate/soften on the surface under the influence of high temperatures, electrolytes, and rock surface affinity. Relying on their inherent viscoelasticity and deformation ability, they adaptively deform and undergo limited volume expansion at pore throats. This characteristic of "rigid transportation and flexible plugging" enables them to form effective blockages in deep, high-permeability channels through bridging, accumulation, and physical adsorption mechanisms, thereby dynamically adjusting the flow direction of subsequent fluids.

3.4.2. Water Control and Oil Recovery Effect

The curves showing the relationship between injection pressure, production degree, water content, and injection volume in the high- and low-permeability tubes during the oil displacement process are, respectively, shown in Figures 8 and 9. The oil displacement experiment indicates that, in the single water flooding process, the crude oil mainly flows out through the high-permeability tubes, and the production degree of the high-permeability tubes is 8 times higher than that of the low-permeability tubes. After the single water flooding process, the production degrees of the high- and low-permeability tubes were 51.3% and 6.2%, respectively, and the total production degree was 32.1%. The production degree of the low-permeability tube was lower. After injecting CD-PPGs, the production degrees of the high- and low-permeability tubes were 68.9% and 30.7%, respectively, which increased by 17.6% and 24.5%, respectively. After CD-PPG displacement, the total production degree was 52.6%, which was 20.5% higher than that of the single water flooding. After injecting CD-PPGs, the particle-blocking agent could effectively seal the high-permeability channels through bridging and aggregation in the pores. In the subsequent water flooding, the remaining oil in the low-permeability area could be effectively utilized, and the sweep efficiency of the low-permeability area was increased by changing the liquid flow direction [43,44].

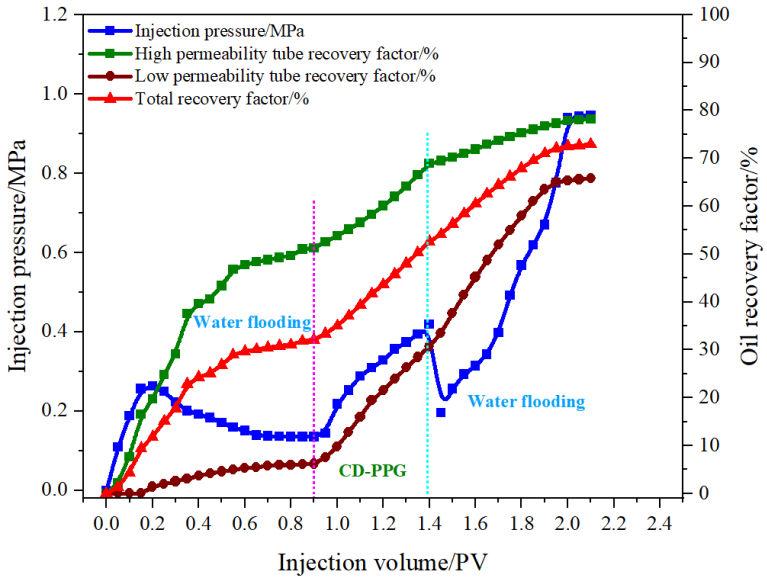


Figure 8. The oil recovery factor and injection pressure curves with injection volume at varying flooding stages.

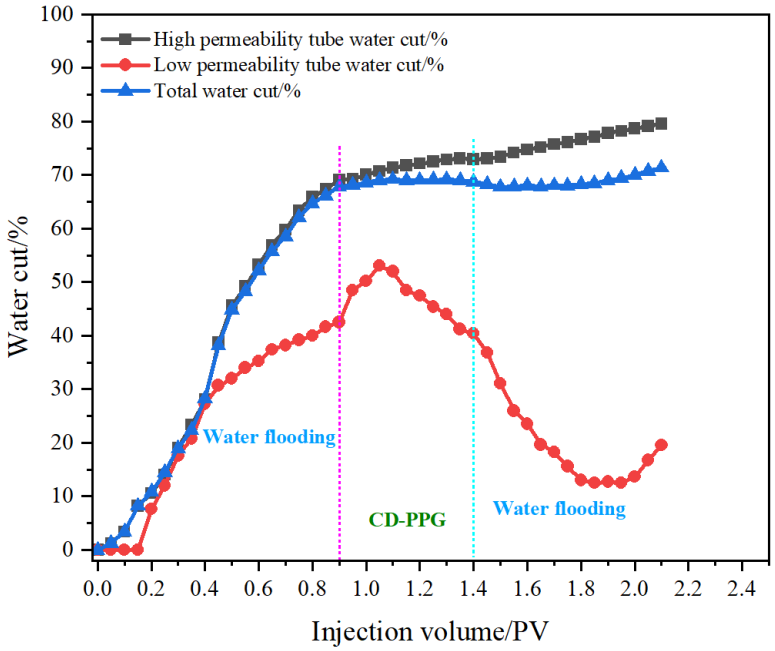


Figure 9. The water cut with injection volume at varying flooding stages.

From Figures 8 and 9, it can be seen that during the first water flooding stage, the water content of the high-permeability wells significantly increased, reaching up to 69.15%, while the water content of the low-permeability wells rose to 41.54%. During this stage, the high-permeability wells had a high production rate, while water migration was severe, whereas the low-permeability wells had a low utilization rate. During the CD-PPG displacement stage, the increase in water content in the high-permeability wells slowed down significantly, while the water content in the low-permeability wells first rose and then dropped. The CD-PPGs entered the flowing channel and preferentially blocked the high-permeability pores and throats [39]. Therefore, during the early stage of gel particle displacement, the water content of the low-permeability channels continued to rise. After the gel particles entered the hypotonic tube, the water content dropped sharply, and the degree of crude oil utilization significantly increased. After the high-permeability pores and throats were blocked, the gel particle displacement stage could more effectively activate the low-permeability well's crude oil, resulting in an increase in crude oil content in the produced fluid and a decrease in water content. During the secondary water flooding stage, the gel particles migrated towards the deeper part of the reservoir through compression deformation. After achieving secondary sealing, the water saturation of the high-permeability zones showed a relatively small increase, while the water saturation of the low-permeability zones first decreased and then rose. Compared with the hypertonic pipe, the low-hypertonic pipe had a smaller amount of gel particles. After long-term flushing, some of the gel particles were extracted, resulting in a reduced effect of profile adjustment and water control. Therefore, after an injection volume of 2.0 PV, the water content of the low-hypertonic pipe increased. CD-PPGs could effectively control water production and enhance the oil recovery rate under heterogeneous reservoir conditions [23,37].

This study designs the moderate crosslinking degree and elastic modulus of particles, making their particle size distribution slightly larger than the mainstream pore throat size in a deep target reservoir. This design has the following rationale: (a) Particles are not rigid spheres. Good deformability allows them to pass through throats slightly smaller than their particle size by 'squeezing deformation' and to partially restore their shape after passing through. (b) Deep plugging mainly occurs at abrupt changes in pore-throat structure or by the bridging and accumulation of multiple particles in larger pore spaces. This kind

of plugging is permeability-dependent; that is, the high-permeability channels that fluids preferentially enter due to their fast flow rate and large throats are more likely to capture and accumulate particles, thereby forming stronger flow resistance and achieving fluid flow diversion. In contrast, low-permeability areas, with their small throats, are less likely to have particles entering or passing through quickly and thus are less affected. Therefore, the seemingly contradictory concepts of "larger-sized particles" and "deep migration plugging" are unified through the deformability of particles and the heterogeneity of formation permeability.

4. Conclusions

In this work, amphiphilic carbon dots (A-CDs) were introduced into the synthesis system of pre-crosslinked gel particles (PPGs), successfully developing a CD-PPG system with self-aggregation characteristics. The following main conclusions were achieved:

(1) A novel PPG based on a dual crosslinking network of "hydrogen bonding—hydrophobic association" was successfully developed, which significantly improved the temperature and salt resistance as well as the mechanical stability of the particle plugging agent. At 110 °C and a salinity of 15×10^4 mg/L, CD-PPGs began to aggregate after aging for 3 days, forming viscoelastic gel clusters, effectively enhancing the plugging capacity of the particle system in porous media.

(2) Under simulated heterogeneous reservoir conditions with permeabilities ranging from 539.0 to 2988.6 mD, the plugging efficiency of 0.5 PV CD-PPGs was above 95%. The gel particles could achieve secondary plugging by migrating deep into the reservoir under pressure deformation, and they had good anti-erosion stability.

(3) Under simulated heterogeneous reservoir conditions with permeabilities of 490.1 mD and 3020.5 mD, the total recovery after displacement by CD-PPGs was 52.6%, which was 20.5% higher than that of primary water flooding. During secondary water flooding, the expansion of gel particles in the pores could effectively plug high-permeability channels, increase the sweep efficiency, and, through fluid flow diversion, enhance the oil recovery efficiency in low-permeability zones.

Author Contributions: Conceptualization, G.X. and T.W.; methodology, X.L.; validation, J.Y. and X.W.; formal analysis, C.T.; investigation, C.T. and T.W.; resources, X.W.; data curation, G.X.; writing—original draft preparation, T.W.; writing—review and editing, J.Y. and X.L. All authors have read and agreed to the published version of the manuscript.

Funding: This research was funded by Tianjin Key Laboratory of Offshore Difficult to Recovery Reserves Exploitation Open Research Project (202516411500).

Data Availability Statement: Data are contained within the article.

Acknowledgments: The authors would like to extend their heartfelt thanks to Yangtze University for the invaluable educational foundation and academic support that have significantly contributed to the development of this work, and express their sincere gratitude to China Oilfield Service Limited for their material support and for providing access to laboratory facilities that were essential for the successful completion of this study. Additionally, the authors also express their sincere appreciation to the anonymous reviewers for their valuable and constructive comments.

Conflicts of Interest: Authors Guorui Xu, Xiaoxiao Li, Jinzhou Yang, Chunyu Tong, and Xiaolong Wang were employed by the China Oilfield Service Limited. The remaining authors declare that the research was conducted in the absence of any commercial or financial relationships that could be construed as a potential conflict of interest.

References

1. Song, T.; Bai, B.J.; Huang, R.; Zhang, S.; Liu, P.D.; Eriyagama, Y.; Tian, X.Y.; Ahdaya, M.; Schuman, T. Development and evaluation of lysine-crosslinked re-crosslinkable particle gel for water control in high-temperature reservoirs. *J. Mol. Liq.* **2024**, *407*, 125133. [CrossRef]
2. Li, M.; Gong, W.H.; Wang, F.; Li, L.; Nie, Y.H.; Chen, Q.B. A novel carbon dot-based degradable preformed particle gel for sensitive detection of iron ions. *Colloids Surf. A* **2025**, *711*, 136414. [CrossRef]
3. Lai, N.J.; Chen, S.F.; Tang, L.; Huang, Y.J.; Xu, H.W. Migration characteristics and profile control capabilities of preformed particle gel in porous media. *Petroleum* **2022**, *8*, 483–498. [CrossRef]
4. Zhu, D.Y.; Zhang, H.J.; Qin, J.H.; Zhao, Q.; Wang, G.Q.; Su, Z.H.; Shi, C.Y. Experimental evaluation of temporary plugging performance and mechanism analysis of degradable preformed particle gel based on NMR technology. *Geoenergy Sci. Eng.* **2025**, *244*, 213480. [CrossRef]
5. Rezaei, A.; Khodabakhshi, A.; Esmaeili, A.; Razavifar, M. Effects of initial wettability and different surfactant-silica nanoparticles flooding scenarios on oil-recovery from carbonate rocks. *Petroleum* **2022**, *8*, 499–508. [CrossRef]
6. Du, L.; Xiao, Y.Y.; Jiang, Z.C.; Zeng, H.B.; Li, H.Z. High-temperature stable dispersed particle gel for enhanced profile control in carbon capture, utilization, and storage (CCUS) applications. *Engineering* **2025**, *48*, 128–140. [CrossRef]
7. Li, W.Z.; Luo, P.Y.; Wang, X.D. Preparation and performance evaluation of graphene oxide-based self-healing gel for lost circulation control. *Polymers* **2025**, *17*, 1999. [CrossRef]
8. Jin, F.Y.; Jiang, T.T.; Varfolomeev, M.A.; Yuan, C.D.; Zhao, H.Y.; He, L.; Jiao, B.L.; Du, D.J.; Xie, Q. Novel preformed gel particles with controllable density and its implications for EOR in fractured-vuggy carbonated reservoirs. *J. Pet. Sci. Eng.* **2021**, *205*, 108903. [CrossRef]
9. Li, M.; Liu, J.; Xia, Y. Risk prediction of gas hydrate formation in the wellbore and subsea gathering system of deep-water turbidite reservoirs: Case analysis from the South China Sea. *Reserv. Sci.* **2025**, *1*, 52–72. [CrossRef]
10. Wu, W.P.; Hou, J.R.; Qu, M.; Yang, Y.L.; Zhang, W.; Wu, W.M.; Wen, Y.C.; Liang, T.; Xiao, L.X. A novel polymer gel with high-temperature and high-salinity resistance for conformance control in carbonate reservoirs. *Pet. Sci.* **2022**, *19*, 3159–3170. [CrossRef]
11. Wang, L.L.; Wang, T.F.; Wang, J.X.; Tian, H.T.; Chen, Y.; Song, W. Enhanced oil recovery mechanism and technical boundary of gel foam profile control system for heterogeneous reservoirs in Changqing. *Gels* **2022**, *8*, 371. [CrossRef] [PubMed]
12. Pu, J.Y.; Johnston, K.P.; Wu, P.; Ahmad, M.; Luo, M.L.; Zhang, N.; He, J.T. Facile synthesis of chromium chloride/poly(methyl methacrylate) core/shell nanocapsules by inverse miniemulsion evaporation method and application as delayed crosslinker in secondary oil recovery. *Pet. Sci.* **2023**, *20*, 396–406. [CrossRef]
13. Kurnia, I.; Fatchurrozi, M.; Anwary, R.; Zhang, G. Lessons learned from coreflood experiments with surfactant-polymer and alkali-surfactant-polymer for enhanced oil recovery. *Petroleum* **2023**, *9*, 487–498. [CrossRef]
14. Liu, Q.; Zhou, K.M.; Liu, Y.J.; Zhang, Y.F.; Chen, W.; Tang, S. Exploring the potential applications of amphiphilic carbon dots based nanocomposite hydrogel in liquid chromatographic separations. *Anal. Chim. Acta* **2024**, *1299*, 342445. [CrossRef]
15. Gao, P.L.; Xie, Z.G.; Zheng, M. Small nanoparticles bring big prospect: The synthesis, modification, photoluminescence and sensing applications of carbon dots. *Chin. Chem. Lett.* **2022**, *33*, 1659–1672. [CrossRef]
16. Cai, M.X.; Lai, L.; Zhao, M.W. Synthesis, properties, and applications of amphiphilic carbon dots: A review. *Carbon* **2025**, *233*, 119921. [CrossRef]
17. Xiao, C.Q.; Wu, J.; Lai, L. Demicellization thermodynamics of amphiphilic carbon dots via isothermal titration calorimetry. *Thermochim. Acta* **2025**, *745*, 179935. [CrossRef]
18. Cao, L.; Lv, M.; Li, C.; Sun, Q.; Wu, M.; Xu, C.; Dou, J. Effects of crosslinking agents and reservoir conditions on the propagation of fractures in coal reservoirs during hydraulic fracturing. *Reserv. Sci.* **2025**, *1*, 36–51. [CrossRef]
19. Zhao, M.W.; Yang, X.Y.; Ma, Z.F.; Li, Y.; Meng, X.J.; Dai, C.L.; Wang, Y.N. A novel nanosurfactant for EOR: Amphiphilic carbon quantum dots (ACDs). *Langmuir* **2025**, *41*, 24004–24015. [CrossRef] [PubMed]
20. Sazzad Parveg, A.S.M.; Zhou, Y.Q.; Leblanc, R.M.; Ratner, A. Effects of gel-like carbon dots (G-CDs) and surfactant (Span80) on the droplet combustion dynamics of liquid fuels. *Fuel* **2025**, *381*, 133385. [CrossRef]
21. Zhai, Y.Y.; Fang, Z.; Feng, J.; Sun, C.J.; Deng, W.J.; Wen, Y.B. Development and performance evaluation of re-crosslinkable preformed particle gel under high temperature and high salt conditions. *Polymer* **2024**, *296*, 126824. [CrossRef]
22. Yang, C.H.; Xiao, D.; Wang, J.; Liang, T. Evaluation and experiment of high-strength temperature- and salt-resistant gel system. *Gels* **2025**, *11*, 669. [CrossRef]
23. Amraeiniya, A.; Shojaei, S.; Mohseni, A.; Mahani, B.; Saatchi, S.; Bahari, A.; Sisakht, S. Experimental study on nanoparticles-assisted low-salinity water for enhanced oil recovery in asphaltenic oil reservoirs. *Petroleum* **2023**, *9*, 395–402. [CrossRef]
24. Liang, L.; Li, J.L.; Li, D.X.; Xu, J.; Zheng, B.; Zhao, J.K. Urea delays high-temperature crosslinking of polyacrylamide for in situ preparation of an organic/inorganic composite gel. *Gels* **2025**, *11*, 256. [CrossRef]

25. Zhou, G.W.; Zhang, X.; Yan, W.J.; Qiu, Z.S. Synthesis, characteristics, and field applications of high-temperature and salt-resistant polymer gel tackifier. *Gels* **2025**, *11*, 378. [CrossRef]
26. Jia, H.; Chen, H.; Zhao, J.Z. Development of a highly elastic composite gel through novel intercalated crosslinking method for wellbore temporary plugging in high-temperature reservoirs. *SPE J.* **2020**, *25*, 2853–2866. [CrossRef]
27. Xin, H.; Fang, B.; Yu, L.Y.; Lu, Y.J.; Xu, K.; Li, K.J. Rheological performance of high-temperature-resistant, salt-resistant fracturing fluid gel based on organic-zirconium-crosslinked HPAM. *Gels* **2023**, *9*, 151. [CrossRef] [PubMed]
28. Bai, Y.Y.; Wen, Y.; Pu, W.F.; Fang, W.; Jin, X. Preparation and self-growth characteristics of in situ self-growing dispersed gel system for offshore large-well-distance reservoirs. *ACS Omega* **2025**, *10*, 40450–40459. [CrossRef] [PubMed]
29. Zhang, J.; Liang, D.; Wang, L.Q.; Tang, E.G.; Li, X.J.; Zhao, W.S. Application of horizontal well discontinuous chemical flooding technology in Bohai oilfield. *Front. Energy Res.* **2023**, *10*, 1036835.
30. Xin, X.K.; Liu, Q.; Liu, S.J.; Yu, G.M.; Wan, Q.S. Optimization of gel flooding during the high water cut stage in a conglomerate reservoir of the Xinjiang A Oilfield. *Polymers* **2023**, *15*, 1809. [CrossRef]
31. Ge, L.Z.; Chen, X.M.; Wang, G.; Zhang, G.H.; Li, J.Y.; Liu, Y.; Xiao, L.X.; Wen, Y.C.; Yuan, W.F.; Qu, M.; et al. Analysis of the distribution pattern of remaining oil and development potential after weak gel flooding in the offshore LD Oilfield. *Gels* **2024**, *10*, 236. [CrossRef]
32. Wang, F.; Kobina, F. The Influence of geological factors and transmission fluids on the exploitation of reservoir geothermal resources: Factor discussion and mechanism analysis. *Reserv. Sci.* **2025**, *1*, 3–18. [CrossRef]
33. Xie, K.; Su, C.; Liu, C.L.; Cao, W.J.; He, X.; Ding, H.N.; Mei, J.; Yan, K.; Cheng, Q.; Lu, X.G. Synthesis and performance evaluation of an organic/inorganic composite gel plugging system for offshore oilfields. *ACS Omega* **2022**, *7*, 12870–12878. [CrossRef]
34. Gallego, J.F.; Medina, O.E.; Tengono, J.A.; Mazo, C.; Maya, A.F.; Caro, C.; Cortés, F.B.; Franco, C.A. Demulsification of Water-in-oil emulsion with carbon quantum dot (CQD)-enhanced demulsifier. *Processes* **2025**, *13*, 575. [CrossRef]
35. Qu, J.; Wang, P.; You, Q.; Zhao, G.; Sun, Y.; Liu, Y. Soft movable polymer gel for controlling water coning of horizontal well in offshore heavy oil cold production. *Gels* **2022**, *8*, 352. [CrossRef] [PubMed]
36. Gao, J.; Wang, X.; Zhang, D.; Wang, J. The formation mechanism of residual oil and methods of enhanced oil recovery in a fractured low-permeability metamorphic rock reservoir in Bohai Bay. *Processes* **2024**, *12*, 2281. [CrossRef]
37. Li, Y.; Liu, C.; Zhang, Y.; Xue, B.; Lv, J.; Miao, C.; Li, Y.; Liu, Z. Experimental investigation on the application of polymer agents in offshore sandstone reservoirs: Optimization design for enhanced oil recovery. *Polymers* **2025**, *17*, 673. [CrossRef]
38. Lai, N.; Wang, D.; Wang, J.; Tang, L. Synthesis, optimization, and characterization of fluorescent particle preformed gel. *Energies* **2022**, *15*, 8712. [CrossRef]
39. Rahman, A.; Torabi, F.; Shirif, E. Surfactant and nanoparticle synergy: Towards improved foam stability. *Petroleum* **2023**, *9*, 255–264. [CrossRef]
40. Zhang, L.; Gao, Z.; Liu, Y.; Li, Y.; Zhou, K.; Wang, P.; Zhang, K.; Wang, C.; Zhang, M. Study on rapid screening method for different chemical flooding methods in heavy-oil reservoirs. *Processes* **2025**, *13*, 2992. [CrossRef]
41. Wang, J.; Wang, R.; Liu, P.; Xu, H. Gel-Forming and plugging performance evaluation of emulsion polymer crosslinking system in fractured carbonate rock. *Processes* **2022**, *10*, 1550. [CrossRef]
42. Tang, E.; Zhang, J.; Jin, Y.; Li, L.; Xia, A.; Zhu, B.; Sun, X. Optimization of discontinuous polymer flooding processes for offshore oilfields using a novel PSO–ICA algorithm. *Energies* **2024**, *17*, 1971. [CrossRef]
43. Shen, M.; Qi, L.; Zhang, L.; Ma, P.; Liu, W.; Ngai, T.; Jiang, H. Dual-responsive hybrid microgels enabling phase inversion in pickering emulsions. *Polymers* **2025**, *17*, 2762. [CrossRef] [PubMed]
44. Wang, R.; Wu, H.; Liu, Z.; Wang, H.; Zhang, Y. Development of high-performance composite cementitious materials for offshore engineering applications. *Materials* **2025**, *18*, 3324. [CrossRef]

Disclaimer/Publisher's Note: The statements, opinions and data contained in all publications are solely those of the individual author(s) and contributor(s) and not of MDPI and/or the editor(s). MDPI and/or the editor(s) disclaim responsibility for any injury to people or property resulting from any ideas, methods, instructions or products referred to in the content.